

RESEARCH ARTICLE

Stratus over rolling terrain: Large-eddy simulation reference and sensitivity to grid spacing and numerics

Jan Weinkaemmerer^{1,2}  | Ivan Bařtak Duran^{1,2,3} | Stephanie Westerhuis^{4,5}  | Jurg Schmidli^{1,2}

¹Institute for Atmospheric and Environmental Sciences, Goethe University Frankfurt, Frankfurt, Germany

²Hans Ertel Centre for Weather Research, Offenbach, Germany

³European Centre for Medium-Range Weather Forecasts, Reading, United Kingdom

⁴Center for Climate Systems Modeling, ETH Zurich, Zurich, Switzerland

⁵Federal Office of Meteorology and Climatology, Zurich, Switzerland

Correspondence

Jan Weinkaemmerer, Institute for Atmospheric and Environmental Sciences, Goethe University Frankfurt, Altenhoferallee 1, 60438 Frankfurt, Germany.

Email:

weinkaemmerer@iauw.uni-frankfurt.de

Funding information

Deutsche Forschungsgemeinschaft, Grant/Award Numbers: TRR 301, 428312742; Hans Ertel Centre for Weather Research, Grant/Award Number: 4818DWDP4

Abstract

The formation of low stratus cloud over idealized hills is investigated using numerical model simulations. The main driver for the cloud formation is radiative cooling due to outgoing longwave radiation. Despite a purely horizontal flow, the advection terms in the prognostic equations for heat and moisture produce vertical mixing across the upper cloud edge, leading to a loss of cloud water content. This behavior is depicted via a budget analysis. More precisely, this spurious mixing is caused by the diffusive error of the advection scheme in regions where the sloping surfaces of the terrain-following vertical coordinate intersect the cloud top. This study shows that the intensity of the (spurious) numerical diffusion depends strongly on the horizontal resolution, the order of the advection schemes, and the choice of scalar advection scheme. A large-eddy simulation with 4-m horizontal resolution serves as a reference. For horizontal resolutions of a few hundred meters and simulations carried out with a model setup as used in numerical weather prediction, a strong reduction of the simulated liquid-water path is observed. In order to keep the (spurious) numerical diffusion at coarser resolutions small, at least a fifth-order advection scheme should be used. In the present case, a weighted essentially nonoscillatory scalar advection scheme turns out to increase the numerical diffusion along a sharp cloud edge compared with an upwind scheme. Furthermore, the choice of vertical coordinate has a strong impact on the simulated liquid-water path over orography. With a modified definition of the sigma coordinate, it is possible to produce cloud water where the classical sigma coordinate does not allow any cloud formation.

KEYWORDS

advection, fog, low stratus, resolution, rolling terrain, vertical coordinate

1 | INTRODUCTION

The presence and formation of fog affect the flow and visibility within the atmospheric boundary layer. This influences transportation by air and land, solar power generation, and the dissipation of air pollution. Therefore, it is important to forecast fog accurately (Nemery *et al.*, 2001; Forthun *et al.*, 2006; Gultepe *et al.*, 2007; Köhler *et al.*, 2017; Gultepe *et al.*, 2019). The different kinds of fog are named after the processes that lead to their formation, for example, radiation fog, advection fog, or evaporation–mixing fog (Whiteman, 2000). Radiation fog develops when the near-surface air cools below its dew-point temperature due to outgoing longwave radiation during night-time. Often this fog is lifted up and forms an elevated cloud layer referred to as low stratus (Scherrer and Appenzeller, 2014). For numerical weather prediction (NWP) models, the accurate simulation of fog and low stratus is challenging due to the variety of physical processes involved, occurring on differing spatial and temporal scales, including radiation, local flow, small-scale turbulence, microphysics, and land–atmosphere interaction (e.g., Van der Velde *et al.*, 2010; Steeneveld *et al.*, 2015). These processes are not resolved explicitly on the numerical grid and thus need to be represented by parameterization. NWP studies for radiation fog over flat terrain (Steeneveld *et al.*, 2015; Steeneveld and de Bode, 2018) show a high sensitivity to land-surface physics and parameterized turbulent mixing. Also, the choice of microphysical scheme has been identified as a key element.

More detailed high-resolution studies require the use of large-eddy simulation (LES) techniques with a very high spatial resolution of up to the 1-m scale in order to resolve the energy-containing eddies in the stable boundary layer. This was first done by Nakanishi (2000), who describes the further development of radiation fog after its onset in calm conditions: when the foggy air mass has grown vertically, radiative cooling at the top of the now optically thick fog causes turbulent mixing by negatively buoyant air, leading to the formation of a stronger adiabatic lapse rate within the fog layer (see also Price, 2011; Price, 2019). Also Bergot (2013) observed organized turbulent structures during the evolution of radiation fog, for example, rolls at the top of the fog layer associated with high values of turbulent kinetic energy (TKE). The transition from shallow stably stratified fog to well-mixed radiation fog is also affected by aerosols (Boutle *et al.*, 2018). LES model results are not always found to provide a consistent benchmark for fog prediction (Boutle *et al.*, 2022). However, recent studies (e.g., Smith *et al.*, 2021) show that fog simulation in NWP models profits from an increased resolution of up to 100 m. These

subkilometer-scale NWP models are becoming more and more common in operational use, at least for limited areas (Boutle *et al.*, 2016).

Most existing fog studies are limited to flat terrain, even if surface inhomogeneities are accounted for (Bergot *et al.*, 2015). Only a few LES studies focus on fog or low stratus over complex terrain (Bergot and Lestringant, 2019). However, the NWP representation of low stratus over complex terrain tends to suffer from inaccuracies. Mostly, some kind of terrain-following vertical coordinate system is used to represent orography in NWP models. Schär *et al.* (2002) show how such a coordinate transformation increases the errors of advective transport. In this study, we want to address the issue of erroneously dissipating low stratus, which was investigated by Westerhuis *et al.* (2020) in a NWP study focusing on the Swiss Plateau. The spurious mixing between adjacent levels of the terrain-following vertical coordinate (in this case, the Smooth LEvel VErtical coordinate, SLEVE, Schär *et al.*, 2002; Leuenberger *et al.*, 2010) was identified as the root cause (Westerhuis *et al.*, 2021). Over mountainous terrain, sloping coordinate surfaces intersect the typically flat cloud top of fog and low stratus, leading to an increased mixing between cloudy and cloud-free grid cells, due to the numerical diffusion of the advection scheme. This phenomenon is also observed in other applications of terrain-following coordinates, for example, as spurious diapycnal mixing in ocean models (Marchesiello *et al.*, 2009). An alternative vertical coordinate formulation with a local smoothing of the model levels seems to mitigate the spurious diffusion considerably (Westerhuis and Fuhrer, 2021).

Apart from the vertical coordinate formulation, the impact of the model dynamics on the fog life cycle has received little attention in the literature. Mazoyer *et al.* (2017) analyzed the impact of the dynamics on the microphysics in a LES of a radiation-fog event with 5-m horizontal and 1-m vertical resolution over flat terrain including surface drag by canopy. They compared different momentum advection schemes: a fourth-order centered scheme and two third- and fifth-order implicitly diffusive weighted essentially nonoscillatory (WENO: Shu, 1998) schemes. The different diffusivities of the schemes affected the fog life cycle significantly. In particular, the highly diffusive third-order scheme led to an unrealistic increase in the liquid water path, due to the dissipation of small-scale turbulent structures at the top of the fog layer, resulting in reduced entrainment of dry air.

Upwind advection schemes, being odd-ordered, are inherently diffusive (Hundsdoerfer *et al.*, 1995). A fifth-order upwind scheme, for instance, can be written as a combination of a sixth-order discretization and an

additional sixth-order derivative term. This introduces dissipation, as the sixth-order derivative term acts as an artificial diffusion term with a diffusivity proportional to the Courant number (Wicker and Skamarock, 2002). The dissipation is largest for short wavelengths (i.e., at strong gradients). Also, even-ordered schemes, though nondissipative, do produce numerical errors due to dispersive oscillations, for example, at inversions or strong moisture gradients (Matheou and Teixeira, 2019). This can also augment the spurious dissipation (Pressel *et al.*, 2017). The purpose of WENO schemes is to suppress oscillations and numerical artifacts in nonsmooth regions with discontinuities or sharp gradients, while maintaining a high accuracy of the solution in smooth regions of the flow. In smooth regions, an arbitrarily high accuracy can be achieved. The main idea is to use a weighted combination of several local reconstructions based on different stencils in order to form the final reconstruction. By using nonlinear weights, several lower-order interpolation polynomials are combined into either a higher-order discretization in smooth parts or a lower-order approximation in nonsmooth parts of the solution. Similarly to upwind schemes, WENO schemes also show diffusive properties (Pantano *et al.*, 2007). In the case of LES, the numerical dissipation of the advection scheme combines with the dissipation of the subgrid model. This can affect the results, as long as the simulation is not well resolved (Brown *et al.*, 2000).

Knowing the effect of terrain-following vertical coordinates on fog dissipation over hilly topography, it is still not clear how other numerical aspects like the type of advection scheme and the order of advection influence fog and low cloud simulation over terrain. In this article, we want to investigate this aspect systematically and compare rolling and flat terrain at a range of different horizontal grid spacings, from the meter scale up to 1 km. Another goal is to understand the mechanisms behind spurious cloud dissipation better by performing a detailed budget analysis for heat and moisture, and to quantify the possible improvement achieved by an alternative vertical coordinate formulation. In order to analyze the resolution dependence, multiple idealized simulations of low stratus cloud are carried out over a simplified valley–ridge topography using regular upwind advection schemes and WENO schemes of different order.

This article is structured as follows. In the next section, the budget analysis and the horizontal averaging method are introduced. The experimental setup and numerical model are presented in Section 3. In Sections 4 and 5, the results of the simulations are discussed. Conclusions are given in Section 6.

2 | BUDGET ANALYSIS

2.1 | Flow averaging and decomposition

With the aim of computing statistical quantities like variances and covariances and evaluating the local budgets of heat and water, the flow needs to be decomposed into turbulent fluctuations and a corresponding ensemble mean using averaging operators (Schmidli, 2013). In the simulations with orography, a sinusoidal valley is used, which is oriented along the meridional or y -direction of the domain (see the cross-sections in Figure 1). In both zonal and meridional directions, periodic boundary conditions are imposed, imitating an infinitely long valley. The symmetry of the quasi-two-dimensional setup used in this study simplifies the decomposition of the flow (Weinkaemmerer *et al.*, 2022).

First, the turbulent fluctuations are separated from the mean flow by a Reynolds decomposition. For a quantity $a(x, y, z, t)$, the required ensemble (Reynolds) average is approximated by an average in time and in the along-valley direction:

$$\bar{a}(x, z, t) = \frac{1}{TL_y} \int_{t-T}^t \int_0^{L_y} a(x, y', z, t') dy' dt', \quad (1)$$

where x , y , and z are the eastward, northward, and vertical directions, respectively, and t is time. Note that z denotes the height above the valley floor. We use a time-averaging period of $T = 20$ min as a compromise between accuracy and stationarity. The sampling time is 1 min. L_y equals the meridional domain length. Thus, the flow is decomposed into an ensemble mean part \bar{a} and a local turbulent part a' :

$$a(x, y, z, t) = \bar{a}(x, z, t) + a'(x, y, z, t). \quad (2)$$

For the sake of clarity, subgrid-scale fluctuations not resolved in the LES are not written out here and are treated as being included in the turbulent part. Following the Reynolds averaging rules, the ensemble mean of a product is given by

$$\overline{ab} = \overline{(\bar{a} + a')(\bar{b} + b')} = \bar{a}\bar{b} + \overline{a'b'}. \quad (3)$$

Note that the second-order turbulent fluxes consist of resolved and subgrid parts:

$$\overline{a'b'} = \overline{a'b'}|_{\text{res}} + \overline{a'b'}|_{\text{sgs}}. \quad (4)$$

For the analysis, the subgrid parts are obtained from the LES subgrid turbulence model.

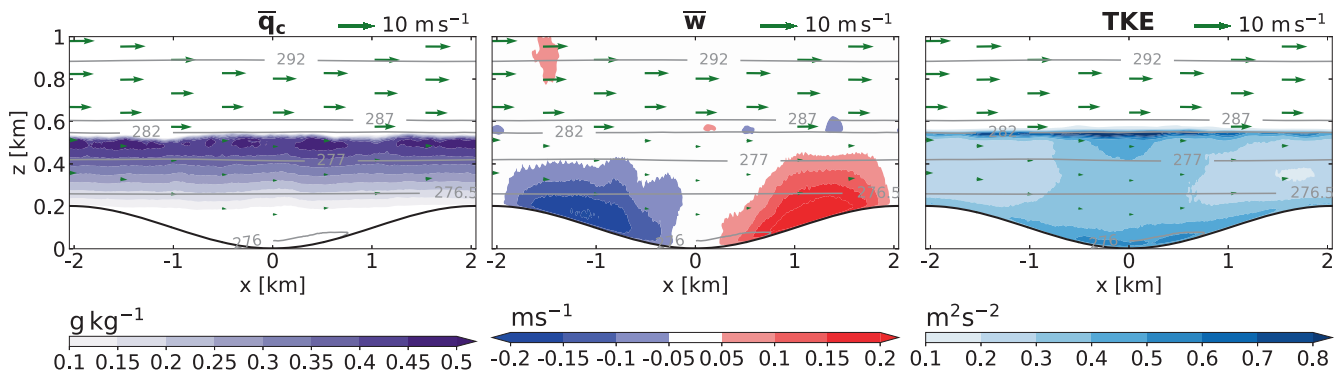


FIGURE 1 Valley cross-sections showing the averaged cloud water content \bar{q}_c , averaged vertical wind speed \bar{w} , and turbulent kinetic energy (TKE) at $t = 6$ hr for the REF case. Also shows the cross-valley wind vectors and the isolines of the potential temperature in K

2.2 | Heat and water budgets

Each term of the conservation equations for heat and water is computed directly from the prognostic equations of the model and averaged as described in Weinkaemmerer *et al.* (2022). This way, the budgets of potential temperature, water-vapor mixing ratio, and cloud water content are obtained. The budgets are comprised of the total tendency (TOT), advection term (ADV), diffusive part of the advection (DIFF), tendencies from the microphysical model (MP), and tendencies from parameterized turbulence, from either the LES subgrid turbulence model or the boundary-layer scheme (PBL) in the NWP case. Additionally, the potential-temperature budget includes a radiation term (RAD).

3 | NUMERICAL MODEL SIMULATIONS

3.1 | Experimental setup

The low stratus case is investigated over a periodic, infinitely long sinusoidal valley. Hence, the setup is quasi-two-dimensional. The orography is described by

$$z_s(x) = \frac{h}{2} \left(1 - \cos \frac{2\pi x}{W} \right), \quad (5)$$

where z_s is the surface height, h the ridge height from valley floor to crest, and W the width of the valley from ridge to ridge. The simulations presented in this study feature a relatively shallow valley with a height h of 200 m and a width W of 4.096 km, which also equals the domain width and length. Rotation is neglected. The initial atmosphere is in hydrostatic balance and the cloud water content is zero everywhere. The initial profiles of temperature, specific

humidity, and wind are loosely derived from a radiosonde sounding launched at Payerne, Switzerland (491 m ASL) on December 25, 2017, at 0000 UTC. An extensive low stratus cloud with a vertical extent of several hundred meters persisted over Payerne on that day; details are described in Westerhuis *et al.* (2020). The initial profiles of potential temperature, water-vapor mixing ratio, and zonal wind are displayed in Figure 2a. A nearly adiabatic residual layer with a moist ground level is capped by a distinct inversion at a height of 500 m. The zonal wind speed increases continuously with height up to $7 \text{ m} \cdot \text{s}^{-1}$ as well as the meridional wind speed (not shown). The wind direction is approximately 45° to the valley axis at all height levels. There is no additional forcing of the flow during the simulation. Radiative forcing is used in combination with an interactive land-surface model. The total duration of the simulations is 6 hr. We lay a special focus on the situation after 6 hr, assuming it to be representative for typical early-morning conditions before sunrise. Thereby, a sufficient amount of time is left for model spin-up. The domain sizes for the experiments are listed in Table 1. In addition to the experiments with orography, several simulations are carried out over a flat surface (FLAT) with the same setup as used over the valley.

3.2 | Numerical model

The numerical simulations are performed using Cloud Model 1 (CM1: Bryan and Fritsch, 2002). CM1 is a nonhydrostatic, fully compressible numerical model that can be run in both LES and NWP modes. It uses terrain-following σ coordinates. This means that the nominal height of a coordinate surface is given by

$$\sigma = \frac{z_t(z - z_s)}{z_t - z_s}, \quad (6)$$

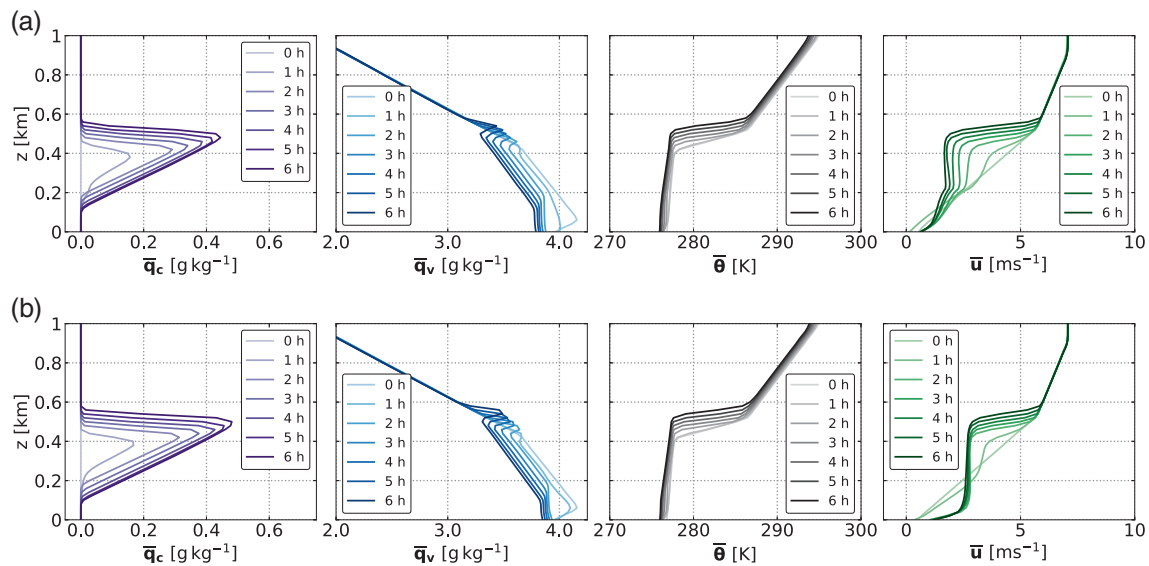


FIGURE 2 Domain-averaged profiles of the cloud water content q_c , water-vapor content q_v , potential temperature θ , and zonal wind u , shown every hour. (a) With orography (REF), height above valley floor; (b) Without orography (FLAT, 8-m horizontal resolution)

TABLE 1 List of model configurations depending on the horizontal resolution

Horizontal resolution	Domain height	Vertical resolution	Subgrid-scale model
4 m	7 km (2-km sponge)	4 m (0–800 m) to 20 m (3.2–7 km)	TKE
8 m	8 km (2-km sponge)	4 m (0–40 m) to 20 m (2.8–8 km)	TKE
16 m	-	-	TKE
32 m	-	-	TKE
64 m	-	8 m (0–40 m) to 40 m (2.8–8 km)	PBL
128 m	-	-	PBL
256 m	-	-	PBL
512 m	-	-	PBL
1,024 m	-	-	PBL

Abbreviations: PBL, Mellor–Yamada Level-3 model (Nakanishi and Niino, 2006); TKE, 1.5-order TKE scheme (Deardorff, 1980).

and depends on the height z , the surface height of the orography $z_s(x, y)$, and the height of the model top z_t . In general, metric terms (G_x , G_y , and G_z) are required to account for this coordinate transformation when calculating spatial gradients, for example, in the advection operator. The model is integrated using third-order Runge–Kutta time differencing (Wicker and Skamarock, 2002). For the default setup, a fifth-order WENO scheme is used for the advection of both scalars and momentum (Jiang and Shu, 1996; Borges *et al.*, 2008). Alternatively, a regular upwind scheme can be used (Wicker and Skamarock, 2002). Grid stretching is applied in the vertical above a certain minimum height. The level thickness increases gradually with altitude (see Table 1). The

model top is a rigid lid. In order to suppress spurious gravity-wave reflections, a sponge layer with Rayleigh damping is employed ($\tau = 300$ s). The model uses an adaptive time step with a typical value of 0.5 s for the LES runs and several seconds for the NWP simulations. At a horizontal resolution of 32 m and below, the simulations are computed in LES mode using a 1.5-order TKE scheme (Deardorff, 1980) for the subgrid-scale turbulence closure. For the NWP simulations, a Mellor–Yamada Level-3 model is used for parameterizing the planetary boundary layer (Nakanishi and Niino, 2006). Microphysical processes are parameterized using the Thompson double-moment scheme (Thompson *et al.*, 2008). Atmospheric radiation is parameterized by the Rapid Radiative Transfer Model

(RRTMG, Iacono *et al.*, 2008). For the land-surface model (revised scheme for the Weather Research and Forecasting model, Jiménez *et al.*, 2012), the grassland option is selected.

4 | DESCRIPTION OF THE LES REFERENCE

In this study, the highest-resolution LES simulation (4-m horizontal resolution) will serve as a reference case (REF) for the following sensitivity tests employing coarser grid spacings. Figure 1 shows cross-sections of the final model state after 6 hr. This is still during night-time, hence the simulations are not affected by solar radiation. An approximately 400-m thick low stratus layer has formed directly above the ridges. The cloud density increases gradually from the bottom to the top of the stratus layer, resulting in a fairly sharp upper cloud edge. The top coincides with a layer of strong wind shear. The mean vertical wind turns out to be negative over the western slope and positive over the eastern slope, indicating that the wind roughly follows the orography. Significant TKE values occur within the stratus layer and in the cloud-free zone at the valley bottom. The TKE is highest along the cloud top, where strong wind shear prevails. A budget analysis for the TKE (not shown) reveals that it is both shear-driven (by the large-scale horizontal wind along the cloud top, as well as by the local surface winds in the valley) and buoyancy-driven (mainly in the center of the domain, due to negatively buoyant air sinking from the cloud top). The averaged subgrid TKE is less than 4% of the total TKE everywhere except in the lowest 50 m of the surface layer.

The temporal evolution of the REF case is displayed in Figure 2a. The cloud water concentration increases gradually with time. Simultaneously, the water-vapor concentration decreases within the stratus layer and also in the cloud-free zone below. Directly above the cloud top, a slight moistening can be observed. With the growth of the stratus layer, the height of the nearly neutrally stratified boundary layer also increases. Due to an overall cooling caused by longwave radiation, the average temperature of the boundary layer decreases over time. During the first hours of simulation, the zonal wind profile in the boundary layer adapts to the nearly adiabatic temperature profile, resulting in an almost constant wind speed between 200 and 500 m and a distinct velocity jump at the inversion height. This shows that the boundary layer is well mixed. For the meridional wind along the valley axis, the temporal evolution is fairly similar, with slightly higher wind speeds inside the valley (not shown).

The evolution of the near-surface atmosphere over flat terrain is qualitatively very similar (Figure 2b). The cloud

water content in the stratus reaches slightly higher values. Furthermore, due to the lack of orographic drag, the wind velocities are higher below 500 m.

5 | SENSITIVITY TO RESOLUTION AND ADVECTION SCHEME

5.1 | Resolution dependence

Figure 3 shows valley cross-sections together with the mean cloud water content at different resolutions. The 32-m simulation was conducted with the LES setup. The coarser the horizontal grid resolution, the thinner and shallower the stratus cloud becomes. At 1024 m, only four grid points are left in the x -direction and the representation of the orography becomes highly nonsmooth. In accordance with the cloud dilution, the temperature inversion below 600 m weakens for coarser resolutions and disappears completely at 1,024 m.

Figure 4 shows the budget terms for the potential temperature, water-vapor content, and cloud water content for the default NWP setup with 256-m horizontal resolution. At this resolution, the effect of spurious diffusion becomes significant. The valley is represented by 16 grid points in the cross-valley direction. Looking at the total tendencies (TOT, upper row), the horizontally homogeneous cooling above the top of the stratus layer is striking, while slightly positive q_c tendencies around 500 m show that the stratus is still growing vertically. The latter are associated with negative q_v tendencies in the same region (partly due to condensation, partly due to growth of the cloud layer) and slightly positive q_v tendencies above. The total θ tendencies are composed of a vertical mixing of heat across the inversion by (implicit numerical) diffusion (ADV+DIFF), leading to a warming around the top of the cloud layer (see dashed line). This local warming is partly balanced by negative θ tendencies from the microphysics (MP) due to evaporation corresponding to negative microphysical tendencies for q_c . Beneath the cloud top (below 500 m), the positive θ tendencies from advection–diffusion, as well as from the microphysics due to condensation, are outweighed by strong radiative cooling (RAD). The PBL tendencies are small for all three quantities.

Areas of nonzero advection–diffusion tendencies in the budgets directly over the slopes and around 900 m height are related to local subsidence (western slope) and ascent (eastern slope, see also Figure 1). Within the stratus, these tendencies are balanced by microphysical processes. Consequently, the vertical transport of θ , q_v , and q_c across the top of the stratus layer must be largely caused by numerical diffusion, as there is no vertical wind present at this height and small-scale turbulent motions

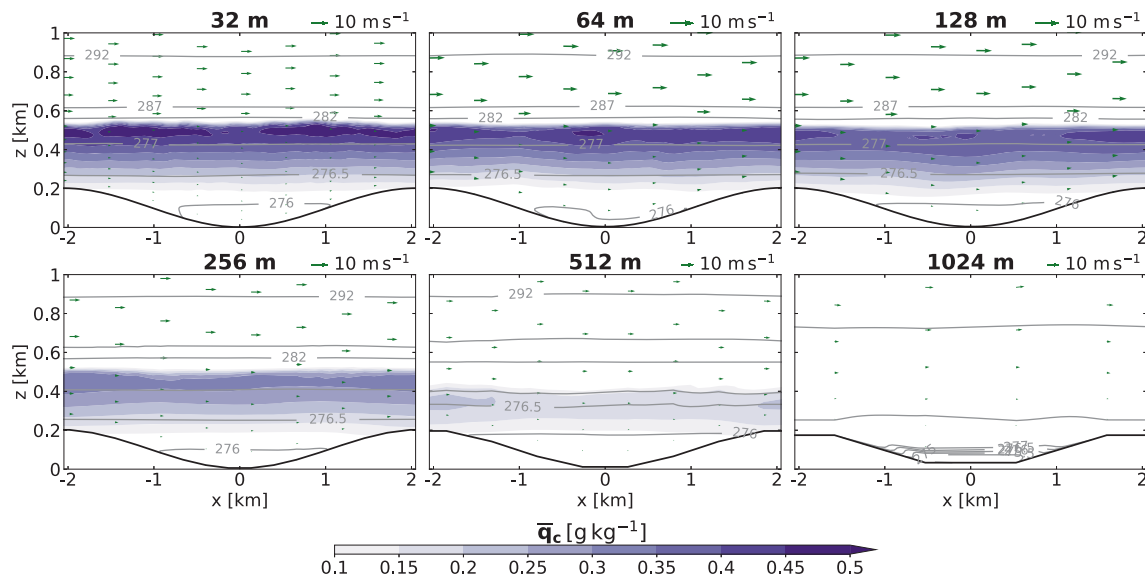


FIGURE 3 Valley cross-sections showing the mean cloud water content for different horizontal resolutions: 32 m (default LES setup) and 64–1,024 m (default NWP setup) at $t = 6$ hr. Also showing the cross-valley wind vectors and the isolines of the potential temperature in K

are not resolved at this resolution. In total, the temperature and moisture gradients at the top of the stratus cloud are still growing, mainly because of strong radiative cooling leading to a gain in q_c due to condensation (see MP in the q_c budget). However, this growth is reduced by numerical diffusion across the cloud top (see ADV+DIFF in the q_c budget). In the q_v budget, the advection–diffusion tendencies are essentially opposite to q_c . Consequently, the microphysical tendencies are also mainly of opposite sign.

The spurious mixing explains why the stratus layer is thinner for coarser resolutions and the boundary layer is generally warmer. The advection–diffusion tendencies around the cloud top reach a maximum over the slopes where the vertical coordinate levels are steepest and the angle between the σ surfaces and the mostly horizontal q_c isosurfaces is highest.

In order to study the impact of the order of advection and type of advection scheme used on cloud evolution, the domain-averaged liquid water path (LWP) is compared for a variety of sensitivity tests over a range of horizontal resolutions (Figure 5a). Over orography, the LWP increases and converges for higher resolutions as the effect of numerical diffusion diminishes. The default simulations have also been carried out over flat terrain for comparison (Figure 5b). Here, the LWP decreases continuously for resolutions higher than 128 m. This opposite behavior is probably due to another effect which dominates over flat terrain in the absence of spurious mixing: resolved small-scale turbulent processes enhance the entrainment of dry air at the top of the stratus layer and

lead to cloud dissipation (Mazoyer *et al.*, 2017). For the default FLAT simulations, the LWP does not converge at high resolutions.

5.2 | Order of advection and WENO

The effective resolution of a model is determined by the smallest resolved wavelength and can be deduced from kinetic energy spectra (Skamarock, 2004). A lower-order advection scheme with increased numerical diffusion results in an overall lower effective resolution. Comparing a third-order scheme for momentum advection with higher-order or central schemes, Lunet *et al.* (2017), and Mazoyer *et al.* (2017), observed an overestimation of the LWP due to enhanced dissipation of TKE reducing the entrainment of dry air at the top of the stratus cloud. Analogously to the resolution dependence, the results are different over the idealized orography of this study, as numerical diffusion is an important factor (Figure 5a). A reduction of the horizontal and vertical advection order from fifth to third order leads to a significant decrease in LWP of sometimes more than 20%. On the other hand, an increase from fifth to seventh order increases the LWP by only a small amount.

In contrast to that, using a fifth-order upwind instead of a fifth-order WENO scheme for scalar advection enhances the amount of cloud water by about 20% on average (Figure 5a). A comparison with a sixth-order centered scheme without implicit diffusion indicates that the fifth-order WENO scheme for scalars is in fact too

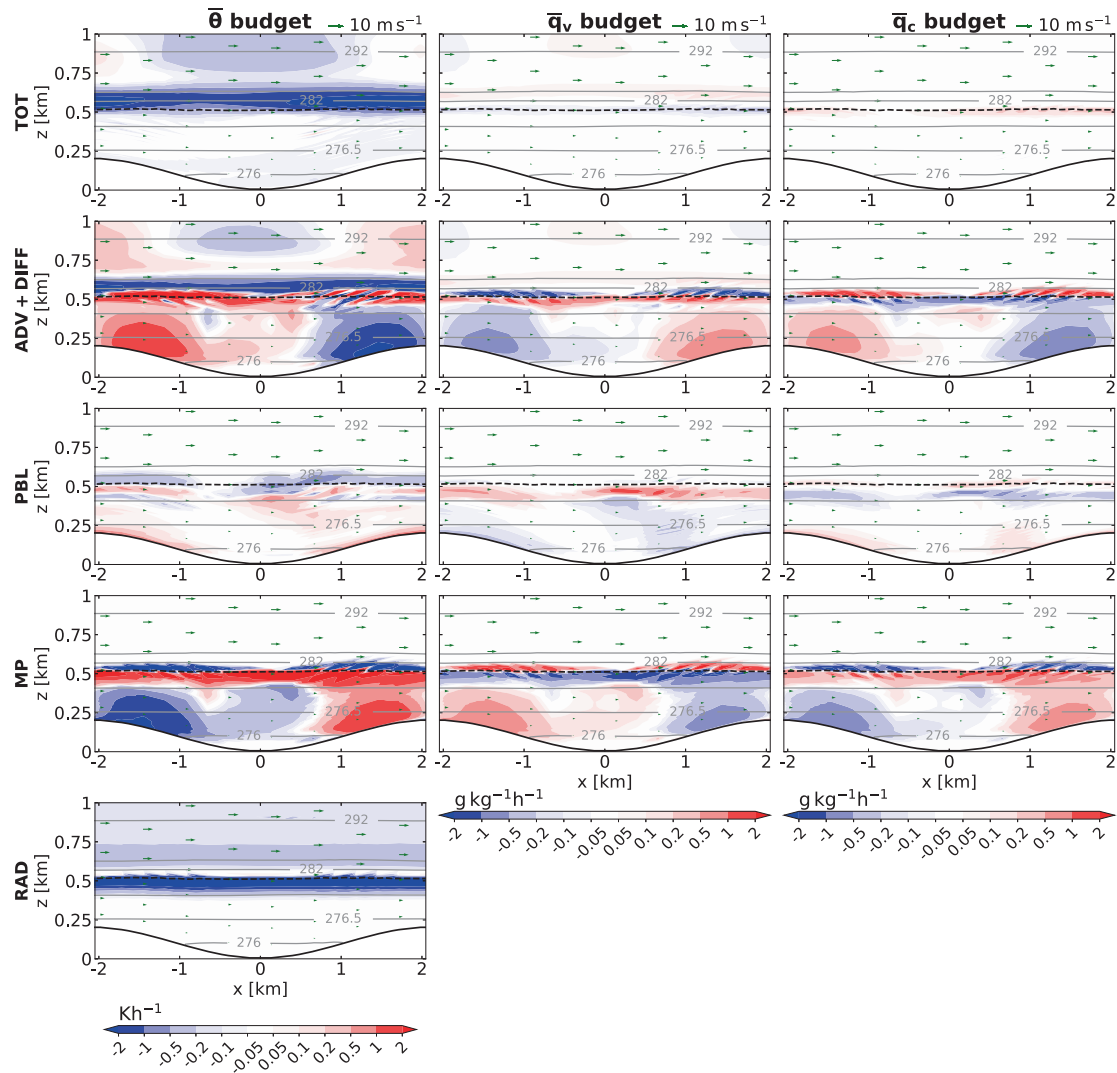


FIGURE 4 Valley cross-sections as in Figure 1, but showing the local budget terms for heat (left column), water vapor (center column), and cloud water (right column) for the default NWP setup with 256 m horizontal resolution at $t = 6$ hr. The budget terms comprise the total tendency (TOT), advection including implicit diffusion (ADV+DIFF), tendencies from the boundary-layer scheme (PBL) as well as the microphysical model (MP), and radiative tendencies (RAD). The dashed black line marks the contour of the cloud top ($0.1 \text{ g} \cdot \text{kg}^{-1}$)

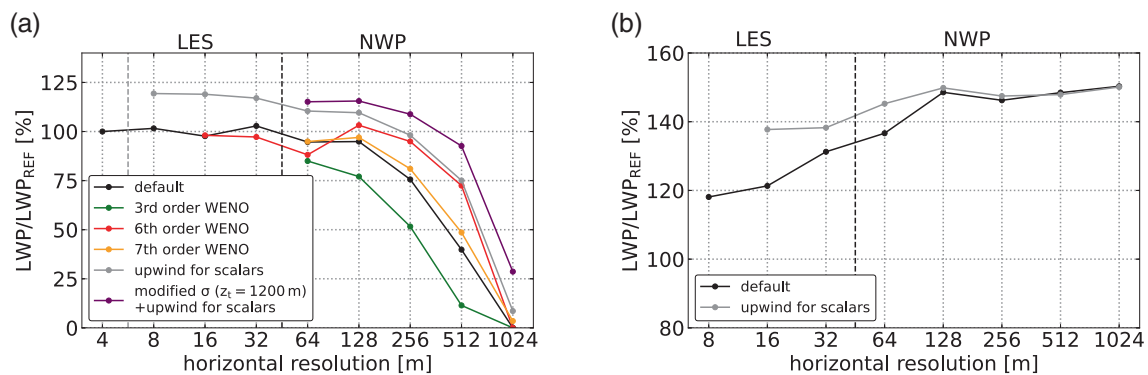


FIGURE 5 Domain-averaged liquid water path (LWP) at $t = 6$ hr obtained from several sensitivity tests for resolution, order of advection, type of advection scheme, and vertical coordinates, both normalized by the LWP of the REF simulation. The dashed black line marks the change from LES to NWP setup (see Table 1). (a) With orography; (b) without orography (FLAT)

diffusive, at least for simulations with grid spacings coarser than 64 m. For the sixth-order simulations, a small amount of artificial sixth-order diffusion was added in order to ensure numerical stability. As a result, this shows that the use of a WENO scheme for scalar advection is not always beneficial around sharp gradients, where it reduces the effective order of advection and thus increases implicit numerical diffusion. At higher resolutions, there is still a systematic discrepancy between the WENO and upwind-scheme simulations, also over flat terrain where no spurious mixing occurs (Figure 5b). Based on this idealized study, we cannot assess finally which results are more realistic. For the FLAT simulations, however, the upwind scheme shows a better convergence at high resolutions and is generally less resolution-dependent.

5.3 | Role of the vertical coordinate

According to Westerhuis and Fuhrer (2021), the effect of spurious numerical diffusion at coarser resolutions associated with the vertical coordinate can be partially mitigated by a stronger damping of the orographic signal with height. Principally, this leads to less steep coordinate surfaces intersecting the flat cloud top. While this can be achieved by a local smoothing of the model levels, this study uses a simpler approach. In Equation (6), z_t is reduced significantly, such that the transition to flat model levels occurs at a lower height. Above z_t , the coordinate levels are completely flat. This implies that the metric term G_z is not independent of height anymore. For $z > z_t$, the metric terms take the values $G_x = G_y = 0$ and $G_z = 1$. For $z_t = 1,200$ m, the effect of this modification can be seen in Figure 5a for the simulations with a fifth-order upwind scheme for scalar advection. The improvement is most significant for coarser resolutions. Even the 1,024-m simulation is able to form a significant amount of cloud water. However, a further decrease of z_t did not lead to a significant further enhancement. This approach has also been tested by Westerhuis *et al.* (2020) by running the Consortium for Small-scale Modeling (COSMO) model over a small, low-altitude region of the Swiss Plateau. The findings are similar but underline the challenging nature of this problem: reducing z_t is only applicable in a domain without high mountains and steep slopes.

6 | CONCLUSION

For this study, idealized simulations of a low stratus event have been carried out over both hilly and flat terrain. The low stratus forms during night-time due to radiative cooling. The sensitivity of the cloud formation with respect to

grid spacing, type of advection scheme for scalars, order of advection, and vertical coordinate formulation has been investigated. The horizontal resolutions cover the full range from a few meters (LES range) to (sub)kilometer NWP resolutions. In terms of scalar advection, WENO schemes of different order have been compared with a regular upwind scheme. The upper cloud edge turns out to be relatively sharp, as it is accompanied by a distinct temperature inversion and a jump in the wind velocity. Terrain-following coordinate levels intersecting the cloud top cause implicit diffusion across the cloud edge, due to the diffusive part of the advection scheme. This leads to spurious mixing, as illustrated with the help of the cloud water budget. In consequence, this results in erroneous cloud dissipation and a reduction of LWP. The main findings from the different sensitivity tests are summarized as follows.

- Over orography, the numerical diffusion associated with the advection of heat and moisture is more resolution-dependent than over flat terrain. While the LWP shows a good convergence in the LES range, it is strongly reduced for coarser resolutions. This originates from the combination of a terrain-following sigma coordinate with a diffusive upwind or WENO advection scheme. For the accurate simulation of fog and low clouds over orography, it is recommended that the relevant orographic features are represented by $\mathcal{O}(30)$ grid points in order to minimize errors due to advection in a terrain-following coordinate system. This means that kilometer-scale NWP simulations are not able to produce accurate results over terrain with orographic features of size several kilometers, for cases comparable with the present one. With an optimized vertical coordinate and higher-order advection scheme, however, reasonable results can be obtained if relevant orographic features are represented by $\mathcal{O}(10)$ grid points.
- The order of scalar advection has a strong impact on the formation of fog and low stratus, especially at resolutions that are actually too coarse for the length-scales of the terrain (see above). For the WENO scheme studied here, an order of five or six seems to be a good compromise. However, a seventh-order scheme does not show a strong improvement compared with a fifth-order scheme. For the case study presented, the WENO scheme in fact turns out to be more diffusive than the regular upwind scheme. Around strong gradients, WENO schemes tend to reduce the effective order of advection in order to avoid oscillations. Over orography, the fifth-order upwind-scheme simulations produce around 20% more LWP than the WENO-scheme simulations over all horizontal resolutions. At low resolutions,

the fifth-order upwind scheme is comparable with the sixth-order scheme, which produces no diffusive errors but rather dispersive ones instead. Based on these findings, an upwind or centered scheme for scalar advection seems to be preferable for cloud simulations with strong gradients. It has to be mentioned that, for momentum advection, a WENO scheme has been used for all simulations in order to avoid numerical instabilities due to the strong wind shear.

- We can confirm that the choice of vertical coordinate has a strong impact on the fog evolution (Westerhuis *et al.*, 2021). Going to higher resolutions in the LES range, the influence of the vertical coordinate decreases. With our simple approach of reducing z_t , so that the model levels become horizontal at a lower height, a considerable increase in LWP could be achieved for the NWP simulations even at the lowest resolution. However, this only works for a domain with rather shallow orography.
- Over flat terrain, the cloud top is aligned with the vertical model levels. Thus, spurious mixing induced by the misalignment of the inversion and the coordinate surfaces does not occur. In this case, the LWP depends on how well small-scale turbulent motions are resolved, which leads to vertical mixing at the cloud top and consequent cloud dissipation. Strong wind shear produces a significant amount of TKE along the cloud top. For the coarser resolutions of the NWP simulations, the turbulent structures disappear in the simulations and the LWP increases. However, with an upwind scheme for scalar advection, the resolution dependence is generally weaker.

It has to be kept in mind that many operational NWP models use different kinds of advection schemes, for example, in order to guarantee positive-definite solutions for tracer transport. These have not been tested here, which is a limitation of this study. More sophisticated vertical-coordinate definitions (Westerhuis and Fuhrer, 2021) are a promising approach to improve the simulation of fog and low stratus over orography. As the cloud top is aligned principally with the isentropes, a hybrid isentropic-sigma vertical coordinate (Toy, 2013) would possibly also help to mitigate the problem of numerical diffusion. The immersed boundary method, currently implemented in the Weather Research and Forecasting (WRF) model (Lundquist *et al.*, 2010), presents another alternative that avoids sloping vertical coordinate levels. However, to our knowledge, WRF is currently the only major NWP model offering this option. Furthermore, concepts like antidiffusive flux corrections for WENO schemes (Xu and Shu, 2005) leave room for future research on the topic of spurious diffusion.

AUTHOR CONTRIBUTIONS

Jan Weinkaemmerer: conceptualization; data curation; formal analysis; investigation; methodology; software; validation; visualization; writing – original draft; writing – review and editing. **Ivan Bařtak Duran:** conceptualization; formal analysis; investigation; methodology; validation. **Stephanie Westerhuis:** formal analysis; investigation; methodology; validation; writing – review and editing. **Jurg Schmidli:** conceptualization; formal analysis; funding acquisition; investigation; methodology; project administration; resources; supervision; validation; writing – review and editing.

ACKNOWLEDGEMENTS

This research was funded by the Hans Ertel Centre for Weather Research of DWD (third phase, The Atmospheric Boundary Layer in Numerical Weather Prediction), Grant Number 4818DWDP4, and by the Deutsche Forschungsgemeinschaft (DFG, German Research Foundation), TRR 301, Project-ID 428312742. Open Access funding enabled and organized by Projekt DEAL.

CONFLICT OF INTEREST

The authors declare no conflict of interests.

ORCID

Jan Weinkaemmerer  <https://orcid.org/0000-0002-1880-4440>

Stephanie Westerhuis  <https://orcid.org/0000-0003-2551-1424>

REFERENCES

- Bergot, T. (2013) Small-scale structure of radiation fog: a large-eddy simulation study. *Quarterly Journal of the Royal Meteorological Society*, 139, 1099–1112.
- Bergot, T., Escobar, J. and Masson, V. (2015) Effect of small-scale surface heterogeneities and buildings on radiation fog: large-eddy simulation study at Paris–charles de gaulle airport. *Quarterly Journal of the Royal Meteorological Society*, 141, 285–298.
- Bergot, T. and Lestringant, R. (2019) On the predictability of radiation fog formation in a mesoscale model: a case study in heterogeneous terrain. *Atmosphere*, 10, 165.
- Borges, R., Carmona, M., Costa, B. and Don, W.S. (2008) An improved weighted essentially non-oscillatory scheme for hyperbolic conservation laws. *Journal of Computational Physics*, 227, 3191–3211.
- Boutle, I., Angevine, W., Bao, J.-W., Bergot, T., Bhattacharya, R., Bott, A., Duconege, L., Forbes, R., Goecke, T., Grell, E., Hill, A., Igel, A.L., Kudzotsa, I., Lac, C., Maronga, B., Romakkaniemi, S., Schmidli, J., Schwenkel, J., Steeneveld, G.J. and Vie, B. (2022) Demistify: a large-eddy simulation (les) and single-column model (scm) intercomparison of radiation fog. *Atmospheric Chemistry and Physics*, 22, 319–333.
- Boutle, I., Finnenkoetter, A., Lock, A. and Wells, H. (2016) The London model: forecasting fog at 333 m resolution. *Quarterly Journal of the Royal Meteorological Society*, 142, 360–371.

- Boutle, I., Price, J., Kudzsota, I., Kokkola, H. and Romakkaniemi, S. (2018) Aerosol–fog interaction and the transition to well-mixed radiation fog. *Atmospheric Chemistry and Physics*, 18, 7827–7840.
- Brown, A.R., MacVean, M.K. and Mason, P.J. (2000) The effects of numerical dissipation in large eddy simulations. *Journal of the Atmospheric Sciences*, 57, 3337–3348.
- Bryan, G.H. and Fritsch, J.M. (2002) A benchmark simulation for moist nonhydrostatic numerical models. *Monthly Weather Review*, 130, 2917–2928.
- Deardorff, J.W. (1980) Stratocumulus-capped mixed layers derived from a three-dimensional model. *Boundary-Layer Meteorology*, 18, 495–527.
- Forthun, G.M., Johnson, M.B., Schmitz, W.G., Blume, J. and Caldwell, R.J. (2006) Trends in fog frequency and duration in the Southeast United States. *Physical Geography*, 27, 206–222.
- Gultepe, I., Sharman, R., Williams, P.D., Zhou, B., Ellrod, G., Minnis, P., Trier, S., Griffin, S., Yum, S.S., Gharabaghi, B., Feltz, W., Temimi, M., Pu, Z., Storer, L.N., Kneringer, P., Weston, M.J., Chuang, H.Y., Thobois, L., Dimri, A.P., Dietz, S.J., França, G.B., Almeida, M.V. and Neto, F.L.A. (2019) A review of high impact weather for aviation meteorology. *Pure and Applied Geophysics*, 176, 1869–1921.
- Gultepe, I., Tardif, R., Michaelides, S., Cermak, J., Bott, A., Bendix, J., Müller, M. D., Pagowski, M., Hansen, B., Ellrod, G., W. Jacobs, G. Toth & S. G. Cober, Placeholder Text (2007) Fog research: a review of past achievements and future perspectives. *Pure and Applied Geophysics*, 164, 1121–1159.
- Hundsdoerfer, W., Koren, B., M. van Loon, Verwer, J.G., Placeholder Text (1995) A positive finite-difference advection scheme. *Journal of Computational Physics*, 117, 35–46.
- Iacono, M. J., Delamere, J. S., Mlawer, E. J., Shephard, M. W., Clough, S. A. and Collins, W. D. (2008) Radiative forcing by long-lived greenhouse gases: calculations with the aer radiative transfer models. *Journal of Geophysical Research: Atmospheres* Placeholder Text, 113, D13103.
- Jiang, G.-S. and Shu, C.-W. (1996) Efficient implementation of weighted eno schemes. *Journal of Computational Physics*, 126, 202–228.
- Jiménez, P.A., Dudhia, J., González-Rouco, J.F., Navarro, J., Montávez, J.P. and García-Bustamante, E. (2012) A revised scheme for the wrf surface layer formulation. *Monthly Weather Review*, 140, 898–918.
- Köhler, C., Steiner, A., Saint-Drenan, Y.-M., Ernst, D., Bergmann-Dick, A., Zirkelbach, M., Bouallégué, Z.B., Metzinger, I. and Ritter, B. (2017) Critical weather situations for renewable energies—part b: low stratus risk for solar power. *Renewable Energy*, 101, 794–803.
- Leuenberger, D., Koller, M., Fuhrer, O. and Schär, C. (2010) A generalization of the SLEVE vertical coordinate. *Monthly Weather Review*, 138, 3683–3689.
- Lundquist, K.A., Chow, F.K. and Lundquist, J.K. (2010) An immersed boundary method for the weather research and forecasting model. *Monthly Weather Review*, 138, 796–817.
- Lunet, T., Lac, C., Auguste, F., Visentin, F., Masson, V. and Escobar, J. (2017) Combination of weno and explicit runge–kutta methods for wind transport in the meso-nh model. *Monthly Weather Review*, 145, 3817–3838.
- Marchesiello, P., Debreu, L. and Couvelard, X. (2009) Spurious diapycnal mixing in terrain-following coordinate models: the problem and a solution. *Ocean Modelling*, 26, 156–169.
- Matheou, G. and Teixeira, J. (2019) Sensitivity to physical and numerical aspects of large-eddy simulation of stratocumulus. *Monthly Weather Review*, 147, 2621–2639.
- Mazoyer, M., Lac, C., Thouron, O., Bergot, T., Masson, V. and Musson-Genon, L. (2017) Large eddy simulation of radiation fog: impact of dynamics on the fog life cycle. *Atmospheric Chemistry and Physics*, 17, 13017–13035.
- Nakanishi, M. (2000) Large-eddy simulation of radiation fog. *Boundary-Layer Meteorology*, 94, 461–493.
- Nakanishi, M. and Niino, H. (2006) An improved mellor–yamada level-3 model: its numerical stability and application to a regional prediction of advection fog. *Boundary-Layer Meteorology*, 119, 397–407.
- Nemery, B., Hoet, P.H. and Nemmar, A. (2001) The meuse valley fog of 1930: an air pollution disaster. *The Lancet*, 357, 704–708.
- Pantano, C., Deiterding, R., Hill, D.J. and Pullin, D.I. (2007) A low numerical dissipation patch-based adaptive mesh refinement method for large-eddy simulation of compressible flows. *Journal of Computational Physics*, 221, 63–87.
- Pressel, K.G., Mishra, S., Schneider, T., Kaul, C.M. and Tan, Z. (2017) Numerics and subgrid-scale modeling in large eddy simulations of stratocumulus clouds. *Journal of Advances in Modeling Earth Systems*, 9, 1342–1365.
- Price, J. (2011) Radiation fog. Part i: observations of stability and drop size distributions. *Boundary-Layer Meteorology*, 139, 167–191.
- Price, J. (2019) On the formation and development of radiation fog: an observational study. *Boundary-Layer Meteorology*, 172, 167–197.
- Schär, C., Leuenberger, D., Fuhrer, O., Lüthi, D. and Girard, C. (2002) A new terrain-following vertical coordinate formulation for atmospheric prediction models. *Monthly Weather Review*, 130, 2459–2480.
- Scherrer, S.C. and Appenzeller, C. (2014) Fog and low stratus over the swiss plateau—a climatological study. *International Journal of Climatology*, 34, 678–686.
- Schmidli, J. (2013) Daytime heat transfer processes over mountainous terrain. *Journal of the Atmospheric Sciences*, 70, 4041–4066.
- Shu, C.-W. (1998) Essentially non-oscillatory and weighted essentially non-oscillatory schemes for hyperbolic conservation laws. In: Quarteroni, A. (Ed.) *Advanced Numerical Approximation of Nonlinear Hyperbolic Equations*. Berlin: Springer, pp. 325–432.
- Skamarock, W.C. (2004) Evaluating mesoscale nwp models using kinetic energy spectra. *Monthly Weather Review*, 132, 3019–3032.
- Smith, D.K., Renfrew, I.A., Dorling, S.R., Price, J.D. and Boutle, I.A. (2021) Sub-km scale numerical weather prediction model simulations of radiation fog. *Quarterly Journal of the Royal Meteorological Society*, 147, 746–763.
- Steenefeld, G., Ronda, R. and Holtslag, A. (2015) The challenge of forecasting the onset and development of radiation fog using mesoscale atmospheric models. *Boundary-Layer Meteorology*, 154, 265–289.
- Steenefeld, G.-J. and de Bode, M. (2018) Unravelling the relative roles of physical processes in modelling the life cycle of a warm radiation fog. *Quarterly Journal of the Royal Meteorological Society*, 144, 1539–1554.
- Thompson, G., Field, P.R., Rasmussen, R.M. and Hall, W.D. (2008) Explicit forecasts of winter precipitation using an improved bulk microphysics scheme. Part ii: implementation of a new snow parameterization. *Monthly Weather Review*, 136, 5095–5115.

- Toy, M.D. (2013) A supercell storm simulation using a nonhydrostatic cloud-resolving model based on a hybrid isentropic-sigma vertical coordinate. *Monthly Weather Review*, 141, 1204–1215.
- Van der Velde, I., Steeneveld, G., Schreur, B.W. and Holtslag, A. (2010) Modeling and forecasting the onset and duration of severe radiation fog under frost conditions. *Monthly Weather Review*, 138, 4237–4253.
- Weinkaemmerer, J., Āurán, I.B. and Schmidli, J. (2022) The impact of large-scale winds on boundary-layer structure, thermally-driven flows, and exchange processes over mountainous terrain. *Journal of the Atmospheric Sciences*.
- Westerhuis, S. and Fuhrer, O. (2021) A locally smoothed terrain-following vertical coordinate to improve the simulation of fog and low stratus in numerical weather prediction models. *Journal of Advances in Modeling Earth Systems*, 13, e2020MS002437.
- Westerhuis, S., Fuhrer, O., Bhattacharya, R., Schmidli, J. and Bretherton, C. (2021) Effects of terrain-following vertical coordinates on simulation of stratus clouds in numerical weather prediction models. *Quarterly Journal of the Royal Meteorological Society*, 147, 94–105.
- Westerhuis, S., Fuhrer, O., Cermak, J. and Eugster, W. (2020) Identifying the key challenges for fog and low stratus forecasting in complex terrain. *Quarterly Journal of the Royal Meteorological Society*, 146, 3347–3367.
- Whiteman, C.D. (2000) *Mountain Meteorology: Fundamentals and Applications*. Oxford: Oxford University Press.
- Wicker, L.J. and Skamarock, W.C. (2002) Time-splitting methods for elastic models using forward time schemes. *Monthly Weather Review*, 130, 2088–2097.
- Xu, Z. and Shu, C.-W. (2005) Anti-diffusive flux corrections for high order finite difference weno schemes. *Journal of Computational Physics*, 205, 458–485.

How to cite this article: Weinkaemmerer, J., Āurán, I.B., Westerhuis, S. & Schmidli, J. (2022) Stratus over rolling terrain: Large-eddy simulation reference and sensitivity to grid spacing and numerics. *Quarterly Journal of the Royal Meteorological Society*, 148(749), 3528–3539. Available from: <https://doi.org/10.1002/qj.4372>